The Astrophysical Journal Letters, 931:L1 (6pp), 2022 May 20 https://doi.org/10.3847/2041-8213/ac6c7f

Radical Recombination during the Phase Transition of Interstellar CO Ice

Jiao He[1], Sándor Góbi[2], Gopi Ragupathy[2], György Tarczay[2,3], and Thomas Henning[1]
[1] Max Planck Institute for Astronomy, Königstuhl 17, D-69117 Heidelberg, Germany; he@mpia.de
[2] MTA-ELTE Lendület Laboratory Astrochemistry Research Group, Institute of Chemistry, ELTE Eötvös Loránd University, H-1518 Budapest, Hungary
[3] Laboratory of Molecular Spectroscopy, Institute of Chemistry, ELTE Eötvös Loránd University, H-1518 Budapest, Hungary
Received 2022 March 2; revised 2022 April 28; accepted 2022 May 4; published 2022 May 18

Abstract

Complex organic molecules (COMs) can be produced efficiently in ice mixtures that simulate the ice mantle on cosmic dust grains, according to prior experimental studies. However, the mechanism that brings the reactive species together in the ice has been debated. Thermal diffusion, which is widely regarded as the main mechanism to bring reactants together, is inefficient at a typical dense cloud temperature of 10 K. A recent experimental study found that the transition of a thin CO ice film from the amorphous to crystalline phase happens at about 10 K. When a small fraction of CO_2 was mixed with CO, the CO_2 molecules can separate and form clusters during CO phase transition. It was further proposed that the separation of minor species in the CO ice during phase transition may be an important mechanism to form interstellar COMs without the need for thermal diffusion. In this study, we try to verify this new mechanism through laboratory experiments. An ice mixture of CH_3OH and CO, which is an analog of the outer layer of the ice mantle on cosmic dust grains, was exposed to UV irradiation to produce radicals such as HCO and CH_2OH, whose concentration was monitored during the subsequent warm-up of the ice. We find clear evidence that during the CO phase transition, most of the radicals recombine to form other molecular species, therefore supporting the recently proposed mechanism of COM formation via CO phase transition.

Unified Astronomy Thesaurus concepts: Interstellar dust (836); Interstellar molecules (849); Molecule formation (2076); Dense interstellar clouds (371); Laboratory astrophysics (2004)

1. Introduction

Ice mantles on cosmic dust grains are the most important factories of interstellar complex organic molecules (COMs; usually defined by astronomers as organic molecules with six or more atoms). So far, over 260 molecules have been identified in the interstellar and circumstellar medium, and most of them are considered COMs.[4,5] Although identified in the gas phase, many of them are formed in ice mantles, because gas-phase reactions are in general much less efficient in forming larger COMs (Öberg 2016). After desorption, either thermally or nonthermally, they are detected by radio telescopes in the gas phase. The presence of many COMs in ice mantles is highly likely. However, due to the difficulty in identifying them in situ in the solid state, only one of them—methanol (CH_3OH)—is securely identified (Chiar et al. 1996; Boogert et al. 2011, 2015). With the James Webb Space Telescope (JWST), the situation will likely change.

Ice mantles have roughly a layered structure (Pontoppidan et al. 2008). The inner layer is dominated by H_2O, CO_2, and NH_3. The outer layer is dominated by CO but also has a significant fraction of CH_3OH and H_2CO to a lesser degree (Boogert et al. 2015). The layered-structure hypothesis has been supported by various observations. In low-mass young stellar objects (YSOs), a large fraction of solid CO_2 is in a water-rich environment, and there exists a high correlation between CO_2 and H_2O, indicating CO_2 is intimately mixed with H_2O in the same layer in the ice mantle (Pontoppidan et al. 2008). This is in agreement with the fact that the formation of both CO_2 and H_2O requires the OH radical and/or O atoms. After the depletion of O atoms (and therefore OH radicals), further freeze-out of CO forms a relatively pure layer of CO outside the H_2O-rich layer. This is supported by the observation of "pure" CO ice in low-mass YSOs (Pontoppidan et al. 2003). Among the two layers, the outer CO-rich layer is particularly important for the formation of COMs. Previous experimental and modeling studies all suggest that many chemical reactions happen in the CO-rich layer to form COMs. From the condensation of atoms (H, C, O, etc.) and simple molecules such as CO and C_2H_2 from the gas phase onto the grain surface, molecules such as CH_4, CH_3OH, formic acid (HCOOH), acetaldehyde (CH_3CHO), glycolaldehyde ($HCOCH_2OH$), ethylene glycol ($(CH_2OH)_2$), and methoxymethanol (CH_3OCH_2OH) are formed from the recombination of radicals in the CO-dominated ice (Fedoseev et al. 2015; Chuang et al. 2016, 2017; Qasim et al. 2019; Chuang et al. 2020; Qasim et al. 2020; Simons et al. 2020; He et al. 2022), and all of these molecules have already been identified in the interstellar medium. When the CH_3OH-containing ice is exposed to electron or UV irradiation, many COMs are produced via radical recombination reactions (Öberg et al. 2009; Maity et al. 2015).

One prerequisite of radical recombination is that a radical has to find another adjacent reaction counterpart so that a chemical reaction is possible. In most gas-grain astrochemical models, the main mechanism for this movement is thermal diffusion (Cuppen et al. 2017). It has been demonstrated that COMs can be formed by radical recombination reactions during the warm-up phase of the cloud (Garrod & Herbst 2006;

[4] D. E. Woon. Interstellar Circumstellar Molecules. http://www.astrochymist.org/astrochymist_ism.html. Last accessed: 2022 February 21.
[5] Molecules in Space. https://cdms.astro.uni-koeln.de/classic/molecules. Last accessed: 2022 February 21.

Garrod et al. 2008). However, thermal diffusion is inefficient under a typical dense cloud temperature of ∼10 K, except for hydrogen. To reconcile the efficient formation of COMs in laboratory experiments with the low thermal diffusion rate, a different mechanism has to be involved. The role of nondiffusive mechanisms has recently been studied in several modeling works (Jin & Garrod 2020; Garrod et al. 2022; Herbst & Garrod 2022), which were based on the assumption that a radical coincidentally sits right next to its reaction counterpart. Without such a coincidence, a question still remains as to how radicals move around in the ice at very low temperatures. This problem was addressed experimentally in a previous study by the Heidelberg group (He et al. 2021).

We found that a $CO:CO_2 = 9:1$ ice mixture undergoes a transition from the amorphous phase to the polycrystalline phase at about 10 K, and during the phase transition CO_2 molecules segregate and form clusters. We quantified the thickness dependence of the phase-transition temperature of pure CO ice and also carried out a whole set of isotherm experiments on 10 monolayers (ML; defined to be 1×10^{15} molecules per cm^2) of $CO:CO_2 = 9:1$ ice mixtures to determine the activation energy of the phase transition. It was found that the phase transition of CO-dominated ice happens at a temperature range typical for dense clouds, and most of the CO-dominated ice in the ice mantle should be polycrystalline. We further proposed that during the phase transition, the minor species buried in the CO ice, including reactive radicals, separate, recombine, and form COMs. We used CO_2 as a proxy of minor species but did not provide direct evidence of radical recombination. The current study fills in the gap and uses an ice mixture of CO and CH_3OH as a representative of the outer layer of the ice mantle and investigates the chemistry triggered by UV irradiation. We provide direct evidence of radical recombination during the phase transition.

The rest of this paper is organized as follows: the experimental setup is described in Section 2, followed by the experimental results and analysis in Section 3. The implications on the formation of COMs and suggested further studies are discussed in Section 4, followed by conclusions in Section 5.

2. Experimental Setup

The experiment was performed using a newly constructed UHV setup, VIZSLA, at ELTE Eötvös Loránd University. A more detailed description is available in a recent review (Bazsó et al. 2021); here we only briefly summarize the main features that are closely related to this study. The main reaction chamber is pumped by a 550 L s^{-1} TURBOVAC MAG W 600 iP turbomolecular pump to a base pressure of 10^{-8} mbar after bake-out at room temperature and to a few 10^{-9} mbar with the cryostat on. Located at the center of the chamber is a gold-coated silver surface, which is used as the substrate onto which ice samples were grown. A closed-cycle helium cryostat (RDK-415D2, Sumitomo Heavy Industries Inc.) can cool the substrate to as low as 3.1 K. A resistive heater installed underneath the substrate can be used to heat the sample up to 300 K. A Lakeshore 336 temperature controller measures and controls the temperature between 3 and ∼300 K to an accuracy of 0.05 K.

Gas mixtures were premixed in a 500 mL glass bulb and then transferred to the substrate through a capillary array doser mounted on a z-manipulator located right in front of the substrate. During the gas deposition, the doser is brought to a distance of approximately 30 mm from the substrate. After deposition, the doser was retracted to allow for free rotation of the substrate.

The mixture of CO and CH_3OH were prepared by first filling the glass bulb with 25 mbar of CH_3OH vapor, followed by 200 mbar of CO. The pressure in the bulb was measured using a capacitance pressure gauge (Pfeiffer CMR 265). To avoid the condensation of CH_3OH on the wall of the stainless tube in the gas manifold, which would affect the mixing ratio, we kept the gas manifold baked at 60° C. The CO gas used in this study is grade 4.7 (Linde) gas. The CH_3OH vapor was evaporated from an HPLC (⩾99.9%) grade liquid after three freeze–pump –thaw cycles to remove dissolved air.

After gas/vapor deposition onto the substrate at 3.1 K and retraction of the doser, the substrate was rotated by 115° to face the hydrogen lamp for UV irradiation. Hydrogen gas flows through a quartz tube surrounded by a microwave cavity to generate plasma. The lamp was powered by using an EMS Microtron 200 Mk3 microwave generator operated at 100 W. The UV light produced from the hydrogen lamp is broadband VUV light dominated by Lyα. The emission profile of a similar lamp has been reported before (Ligterink et al. 2015). The LiF window between the hydrogen lamp and the UHV chamber has a cutoff at 120 nm. An irradiation duration of 30 minutes was chosen for the experiment reported here.

The composition of the mixed ice on the substrate was measured using a Bruker Invenio-R Fourier-Transform Infrared (FTIR) spectrometer in the Reflection Absorption InfraRed Spectroscopy (RAIRS) configuration. The infrared beam is forming a 60° angle with respect to the surface normal. The spectrometer scans 32 times and averages them every 15 s. After irradiation, the ice was heated up at a ramp rate of 2 K $minute^{-1}$, giving a temperature resolution during heating up of 0.5 K.

Although the composition of the gas mixture was determined to be $CH_3OH:CO = 12.5:100$ from the pressure measurement in the bulb, we preferred to use the RAIRS data to estimate the mixing ratio because the pumping speed for CO may be different from that for CH_3OH in the chamber. The absorption bands at ∼2140 cm^{-1} and ∼1030 cm^{-1} are used to calculate the column densities of CO and CH_3OH, with band-strength values of 1.1×10^{-17} (Jiang et al. 1975) and 1.6×10^{-17} (Kerkhof et al. 1999), respectively. Based on this, we calculated the total thickness of the mixed ice to be 580 ML, with a $CH_3OH:CO$ mixing ratio of 7.1:100, lower than the value determined from the pressure measurement. We note that both methods for determining the mixing ratio have some uncertainties. We take the absolute error of the mixing ratio to be less than 50%, which is roughly the difference between the two methods of mixing ratio estimation.

3. Results and Analysis

In the experiment, 580 ML of $CH_3OH:CO = 7.1:100$ mixed ice was deposited onto the substrate while it was at 3.1 K. After deposition, the substrate was rotated to face the hydrogen lamp and exposed to UV irradiation for 30 minutes before returning to its original position for the subsequent warm-up to 40 K at 2 K $minute^{-1}$. Figure 1 shows the RAIRS spectra after deposition at 3.1 K, after UV irradiation at 3.1 K, and at 5.3 and 40.2 K during the warm-up (temperature-programmed desorption, TPD). To show the changes in each feature more clearly, in Figure 2 we selected the most interesting regions and added

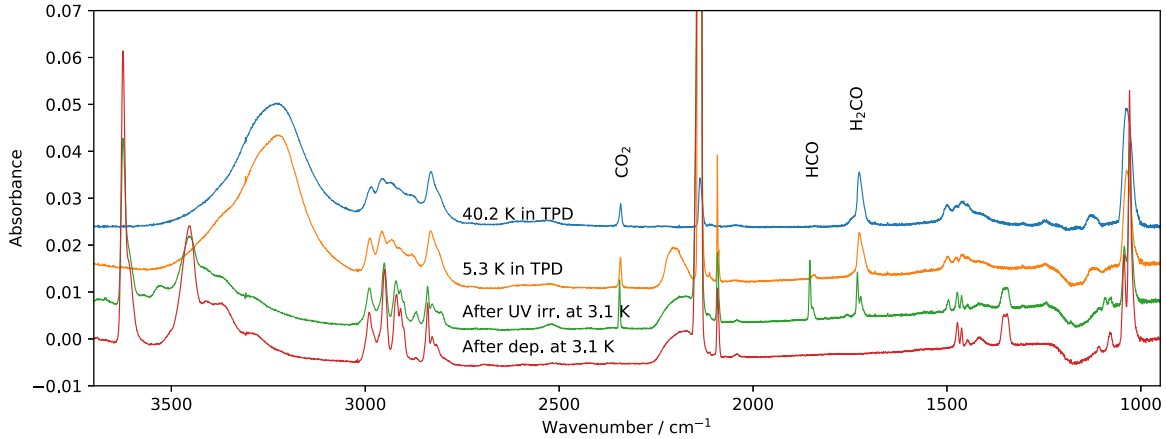

Figure 1. RAIRS spectra of the CH_3OH:CO = 7.1:100 mixed ice: (1) after deposition at 3.1 K, (2) after 30 minutes of UV irradiation at 3.1 K, (3) during the warm-up at 5.3 K, and (4) during the warm-up at 40.2 K. The three newly formed major species, HCO, H_2CO, and CO_2, are labeled in the figure.

more curves during the warm-up. In the following subsections, we analyze the RAIRS spectra of deposited species CO and CH_3OH and of the identified new species CO_2, HCO, H_2CO, and CH_2OH.

3.1. CO and CH_3OH

RAIRS spectra of the CO and CH_3OH mixtures were presented in Maity et al. (2015); our spectra are somewhat different because of a lower concentration of CH_3OH. In the spectrum after deposition, the peaks at $\sim$2140 cm^{-1} and $\sim$2092 cm^{-1} are due to CO and ^{13}CO, respectively. The rest of the peaks are all due to CH_3OH. Phase transition of the ice from amorphous to polycrystalline starts already at 3.8–4.2 K and is most significant between 4.2 and 4.7 K; it is almost complete by 4.7 K. Multiple changes are clearly seen during the phase transition: (a) the CO peak at $\sim$2140 cm^{-1} changes its shape; the transversal optical (TO) mode at 2135 cm^{-1} blueshifts to 2137 cm^{-1}, and the longitudinal (LO) mode at 2143 cm^{-1} becomes smaller; (b) the ^{13}CO peak at 2092 cm^{-1} splits into two peaks at 2092 cm^{-1} and 2088 cm^{-1}, due to LO and TO modes, respectively; this LO–TO splitting is typical in crystalline ices; (c) two main peaks at 3624 and 3455 cm^{-1} merge into a single broad peak at 3230 cm^{-1} attributed to bulk CH_3OH; this feature is typically found in pure CH_3OH ice; it suggests the formation of larger clusters of CH_3OH; the complicated features at 1380–1500 and 2800–3000 cm^{-1} also become less sharp; the peak at 1350 cm^{-1} disappears after the transition. All of these changes support that a phase transition happens between $\sim$4 and 5 K, and minor species in the ice segregate. This is similar to He et al. (2021), in which CO_2 clusters form during the CO phase transition.

3.2. CO_2

The formation of CO_2 is clearly seen from the 2344 cm^{-1} peak. Its formation could be explained by three mechanisms:

1. Photolysis of CH_3OH produced OH radicals, which react with CO to form CO_2 and H atoms (Noble et al. 2011).
2. The OH radical reacts with CO to form the HOCO radical, which again reacts with another H atom to form CO_2 and H_2 (Qasim et al. 2019). The reactions between CO and OH have been proposed to be major sources of CO_2 in the ice mantle on interstellar dust grains, although it is still debated whether the reaction passes through the HOCO radical (Qasim et al. 2019).
3. UV irradiation produces CO in an excited state (CO*), which reacts with another ground-state CO to produce CO_2 and a carbon atom. It is known that the energy of the Lyα radiation emitted by the hydrogen lamp is sufficient to excite CO but insufficient to dissociate it. This explains the formation of CO_2 in experiments where pure CO is exposed to UV, and CO_2 is produced (Loeffler et al. 2005).

The reactions involved are listed below:

$$CH_3OH \xrightarrow{uv} CH_3 + OH, \quad (1)$$

$$CO + OH \rightarrow CO_2 + H, \quad (2)$$

$$CO + OH \rightarrow HOCO, \quad (3)$$

$$HOCO + H \rightarrow CO_2 + H_2, \quad (4)$$

$$CO \xrightarrow{uv} CO^*, \quad (5)$$

$$CO + CO^* \rightarrow CO_2 + C. \quad (6)$$

During the phase transition, the CO_2 peak redshifts from 2344 to 2342 cm^{-1}. In He et al. (2021), when 10% of CO_2 is mixed with CO, the same peak was found to shift to the opposite direction to 2347 cm^{-1} during the CO phase transition. The likely reason for the difference is that in this study, the amount of CO_2 produced by UV is much smaller than CH_3OH; when phase transition pushes the impurities to cluster together, CO_2 predominantly interacts with CH_3OH rather than with other CO_2 molecules. This is even clearer at $\sim$40 K—when most of the CO is already sublimated and the ice is dominated by CH_3OH, the peak is centered at $\sim$2341 cm^{-1} rather than 2347 cm^{-1}.

3.3. HCO and H_2CO

HCO, CH_2OH, and H_2CO are mostly produced by the following reactions:

$$CH_3OH \xrightarrow{uv} CH_3O + H, \quad (7)$$

$$CH_3OH \xrightarrow{uv} CH_2OH + H, \quad (8)$$

$$CH_3O \xrightarrow{uv} H_2CO + H, \quad (9)$$

$$CH_2OH \xrightarrow{uv} H_2CO + H, \quad (10)$$

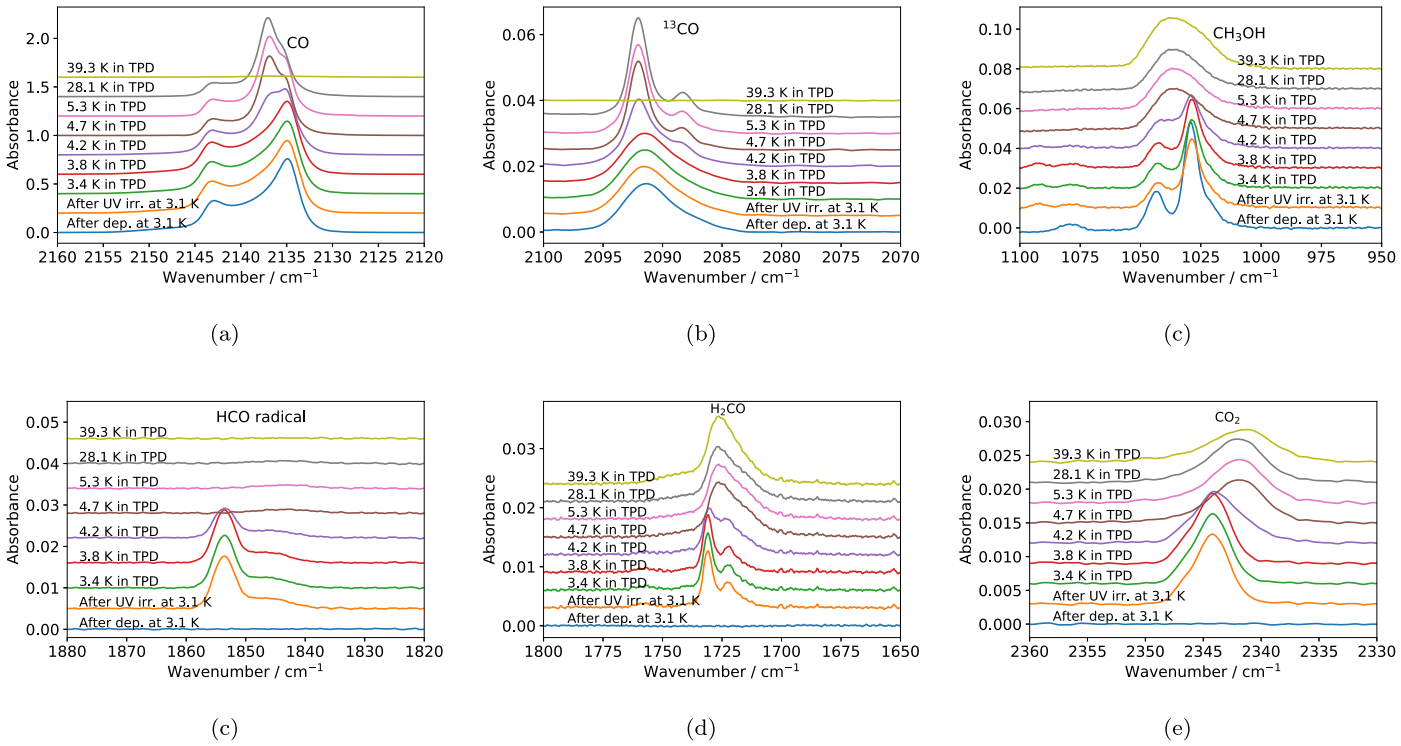

Figure 2. RAIRS spectra of (a) CO, (b) ^{13}CO, (c) CH_3OH, (d) HCO, (e) H_2CO, and CO_2 after deposition at 3.1 K, after UV irradiation at 3.1 K, and at a few selected temperatures (4.2, 4.7, 5.3, 28.1, and 39.3 K) during the subsequent linear warm-up (TPD).

$$H_2CO \xrightarrow{uv} HCO + H, \quad (11)$$

$$CO + H \rightarrow HCO, \quad (12)$$

$$H_2CO + H \rightarrow CH_2OH/CH_3O, \quad (13)$$

$$CH_2OH/CH_3O + H \rightarrow CH_3OH, \quad (14)$$

$$H_2CO + H \rightarrow HCO + H_2, \quad (15)$$

$$CH_3OH + H \rightarrow CH_2OH + H_2, \quad (16)$$

$$HCO + H \rightarrow H_2CO, \quad (17)$$

$$HCO + HCO \rightarrow H_2CO + CO. \quad (18)$$

Among these reactions, those involving a parent species (either CO or CH_3OH) are most important during the irradiation, i.e., reactions (7), (8), and (12). Most of the HCO are produced by reaction (12). The main route of H_2CO formation is less clear. Reactions (9), (10), and (17) are probably the most relevant ones during irradiation. Reaction (10) likely contributes more than reaction (9) because the photolysis of CH_3OH produces more CH_2OH than CH_3O (Öberg et al. 2009). In addition, we have identified CH_2OH, but no evidence of CH_3O. Recombination of radicals other than H during irradiation is not important because of the low concentration and low mobility of radicals at 3.1 K.

During the irradiation phase, the reaction with H is the main destruction route of HCO. During the warm-up, however, the hydrogenation of HCO is much less efficient because of the lack of H atoms. Any H atom that is produced in the irradiation stage should be quickly consumed because H atoms are surrounded by molecules/radicals that they can react with. What remains in the ice after irradiation are only radicals other than H. Therefore, during the subsequent warm-up stage, the main reaction is (18), which consumes HCO to form H_2CO. Figure 2(c) shows that almost all of the HCO is consumed between 4 and 5 K when the phase transition happens.

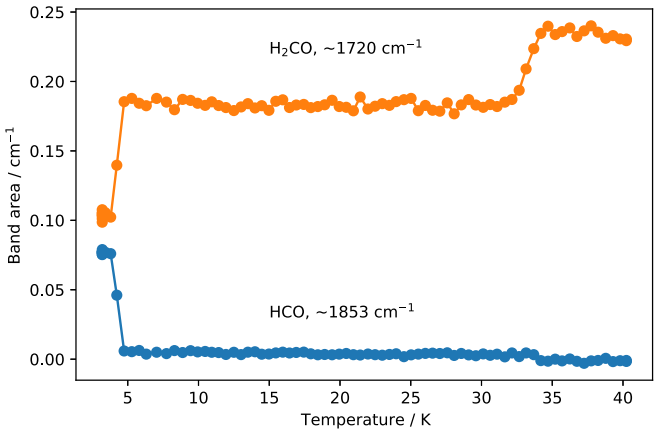

Figure 3. Band area of the HCO and H_2CO absorption peaks at ~1854 and ~1720 cm^{-1}, respectively, during the warm-up of the UV-processed CH_3OH:CO=7.1:100 mixed ice.

Simultaneously, the amount of H_2CO increases. This confirms the recombination of HCO radicals during the phase transition. Figure 3 shows the integrated band area of HCO and H_2CO during the warm-up. Other than the phase transition at 4–5 K, another significant change happens at 32–34 K when most of the CO desorbs. A small amount of remaining unreacted HCO is consumed at this temperature. At the same time, the band area of H_2CO sees a much larger increase, which cannot be explained by reaction (18). This is likely because H_2CO has a larger absorption band strength in a CH_3OH- or H_2CO-rich environment than in a CO-rich environment.

We attributed the ~1720 cm^{-1} peak to H_2CO. However, it is also possible that a small fraction of other molecules is contributing to this peak, such as CH_3CHO, CH_3OCHO,

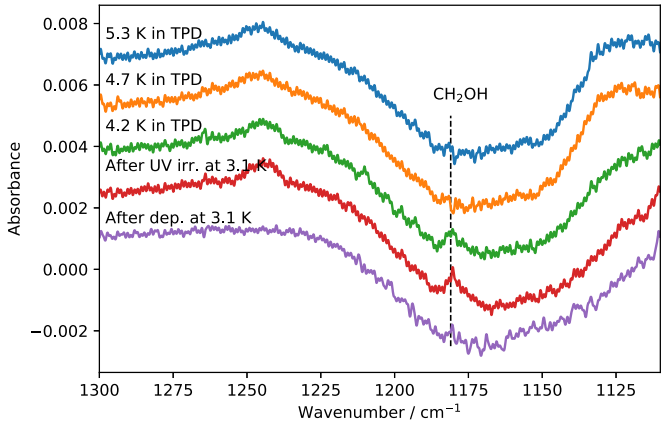

Figure 4. RAIRS spectra of CH_3OH:CO = 7.1:100 mixed ice between 1110 and 1300 cm^{-1}: (1) after deposition at 3.1 K; (2) after 30 minutes of UV irradiation at 3.1 K; and (3) during the warm-up (TPD) at 4.2, 4.7, and 5.3 K. The expected position of CH_2OH absorption is marked.

CH_2OHCHO, etc. Further experiments with better precision would be required to identify these species.

3.4. CH_2OH

CH_2OH is one of the main photolysis products of CH_3OH (Öberg et al. 2009), as well as a product of hydrogen abstraction of CH_3OH (Hidaka et al. 2009; Lee et al. 2015; Chuang et al. 2016). We found evidence for CH_2OH as shown in Figure 4. After irradiation, a small peak at 1181 cm^{-1} shows up. This is attributed to the CH_2OH radical (Jacox 1981; Bennett et al. 2007). It disappears during the phase transition at 4–5 K. This suggests that when the CO phase transition happens, CH_2OH radicals react with other radicals such as HCO to form COMs containing two carbon atoms.

4. Discussion

It is clear from the experimental result that HCO and CH_2OH radicals are produced by UV irradiation, and most of these radicals are consumed during the phase transition at 4–5 K. The small fraction of unreacted ones remain in the ice until the desorption of the CO matrix, and then they fully react. In a realistic ice mantle, the minor species in the CO ice are not limited to HCO and CH_2OH; other radicals, such as CH_3O, CH_3, CH_2, CH, C, O, and OH, and even nitrogen-containing species may also be present. These radicals could be condensed directly from the gas phase, formed in the solid state by thermal reactions, or produced by irradiation. The recombination of them is likely to happen during the CO phase transition as well.

In the experiment of this study, the 580 ML CH_3OH:CO = 7.1:100 mixed ice undergoes a phase transition at 4–5 K. This is lower than the transition temperature reported in He et al. (2021) for much thinner CO:CO_2 mixed ices. He et al. (2021) have already shown that the phase-transition temperature depends on ice thickness. Accordingly, it is expected that similar recombination reactions can take place at slightly higher temperatures in thinner ices, the temperatures of which are more relevant in a real astrophysical environment. It is also likely to depend on the composition of the ice. Future laboratory work should be done to quantify the thickness and composition dependence of the phase transition. In this study, the phase transition occurs at 4–5 K, which is not representative of molecular clouds. This is due to the large thickness being employed. However, the proposed COM formation mechanism by radical recombination during the CO phase transition should nevertheless apply to realistic molecular cloud conditions where the CO thickness is only a few MLs and the phase-transition temperature is between a few Kelvin to 20 K, representative of molecular clouds (Boogert et al. 2015; He et al. 2021).

Experimental studies involving CO-containing ice, such as the hydrogenation of CO, or the energetic processing of CO-containing ice mixture, should consider the role of CO phase transition. Notably, it is worth performing the experiments at a temperature lower than the phase-transition temperature to find out the role of phase transition.

5. Conclusions

One of the fundamental questions regarding the formation of COMs in ices is how reactants, particularly radicals, move in the ice and meet the other reaction counterpart. In this study, we exposed a CO and CH_3OH mixed ice to UV to study the fate of radicals during the subsequent thermal processing of the ice. We found clear evidence that radical recombination happens during the amorphous to the polycrystalline phase transition of the CO-dominated ice mixture at temperatures as low as 4–5 K. In realistic interstellar ice, the thickness of CO is much smaller, and it is expected that similar recombination reactions can take place at a slightly higher temperature, closer to that of the real astrophysical environment. Our results provide direct experimental support that radical recombination during the CO-ice phase transition could be one of the most important mechanisms for forming COMs in the interstellar medium.

The support of the Lendület program of the Hungarian Academy of Sciences is acknowledged. This work was also supported by the ELTE Institutional Excellence Program (grant TKP2021-NKTA-64). J.H. and T.H. acknowledge support from the European Research Council under the Horizon 2020 Framework Program via the ERC Advanced Grant Origins 83 24 28.

ORCID iDs

Jiao He https://orcid.org/0000-0003-2382-083X
Sándor Góbi https://orcid.org/0000-0002-7039-8099
György Tarczay https://orcid.org/0000-0002-2345-1774
Thomas Henning https://orcid.org/0000-0002-1493-300X

References

Bazsó, G., Csonka, I. P., Góbi, S., & Tarczay, G. 2021, RScI, 92, 124104
Bennett, C. J., Chen, S.-H., Sun, B.-J., Chang, A. H. H., & Kaiser, R. I. 2007, ApJ, 660, 1588
Boogert, A. C. A., Gerakines, P. A., & Whittet, D. C. B. 2015, ARA&A, 53, 541
Boogert, A. C. A., Huard, T. L., Cook, A. M., et al. 2011, ApJ, 729, 92
Chiar, J. E., Adamson, A. J., & Whittet, D. C. B. 1996, ApJ, 472, 665
Chuang, K.-J., Fedoseev, G., Ioppolo, S., van Dishoeck, E. F., & Linnartz, H. 2016, MNRAS, 455, 1702
Chuang, K.-J., Fedoseev, G., Qasim, D., et al. 2017, MNRAS, 467, 2552
Chuang, K. J., Fedoseev, G., Qasim, D., et al. 2020, A&A, 635, A199
Cuppen, H. M., Walsh, C., Lamberts, T., et al. 2017, SSRv, 212, 1
Fedoseev, G., Cuppen, H. M., Ioppolo, S., Lamberts, T., & Linnartz, H. 2015, MNRAS, 448, 1288
Garrod, R. T., & Herbst, E. 2006, A&A, 457, 927
Garrod, R. T., Jin, M., Matis, K. A., et al. 2022, ApJS, 259, 1
Garrod, R. T., Widicus Weaver, S. L., & Herbst, E. 2008, ApJ, 682, 283

He, J., Simons, M., Fedoseev, G., et al. 2022, A&A, 659, A65
He, J., Toriello, F. E., Emtiaz, S. M., Henning, T., & Vidali, G. 2021, ApJL, 915, L23
Herbst, E., & Garrod, R. T. 2022, FrASS, 8, 209
Hidaka, H., Watanabe, M., Kouchi, A., & Watanabe, N. 2009, ApJ, 702, 291
Jacox, M. E. 1981, CP, 59, 213
Jiang, G. J., Person, W. B., & Brown, K. G. 1975, JChPh, 62, 1201
Jin, M., & Garrod, R. T. 2020, ApJS, 249, 26
Kerkhof, O., Schutte, W. A., & Ehrenfreund, P. 1999, A&A, 346, 990
Lee, Y.-F., Chou, W.-T., Johnson, B. A., et al. 2015, JMoSp, 310, 57
Ligterink, N. F. W., Paardekooper, D. M., Chuang, K. J., et al. 2015, A&A, 584, A56
Loeffler, M. J., Baratta, G. A., Palumbo, M. E., Strazzulla, G., & Baragiola, R. A. 2005, A&A, 435, 587
Maity, S., Kaiser, R. I., & Jones, B. M. 2015, PCCP, 17, 3081
Noble, J. A., Dulieu, F., Congiu, E., & Fraser, H. J. 2011, ApJ, 735, 121
Öberg, K. I. 2016, ChRv, 116, 9631
Öberg, K. I., Garrod, R. T., van Dishoeck, E. F., & Linnartz, H. 2009, A&A, 504, 891
Pontoppidan, K. M., Fraser, H. J., Dartois, E., et al. 2003, A&A, 408, 981
Pontoppidan, K. M., Boogert, A. C. A., Fraser, H. J., et al. 2008, ApJ, 678, 1005
Qasim, D., Fedoseev, G., Chuang, K. J., et al. 2020, NatAs, 4, 781
Qasim, D., Lamberts, T., He, J., et al. 2019, A&A, 626, A118
Simons, M. A. J., Lamberts, T., & Cuppen, H. M. 2020, A&A, 634, A52